Title

Measured Biaxial Residual Stress Maps in a Stainless Steel Weld

Journal

Journal of Nuclear Engineering and Radiation Science, 1(4)

ISSN

2332-8983

Authors

Olson, Mitchell D
Hill, Michael R
Patel, Vipul I
et al.

Publication Date

2015-10-01

DOI

10.1115/1.4029927

Peer reviewed

Measured Biaxial Residual Stress Maps in a Stainless Steel Weld

Mitchell D. Olson[1], Michael R. Hill[1*], Vipul I. Patel[2], Ondrej Muránsky[2], Thomas Sisneros[3]

[1] *Department of Mechanical and Aerospace Engineering, University of California, One Shields Avenue, Davis, CA 95616*

[2] *Institute of Materials Engineering, ANSTO, Kirrawee-Sydney, NSW, Australia*

[3] *Los Alamos Neutron Science Center, Los Alamos National Laboratory, Los Alamos, NM 87545*

Submitted to Journal of Nuclear Engineering and Radiation Science, November 2014
Accepted for Publication, February 2014
http://dx.doi.org/10.1115/1.4029927

ABSTRACT

This paper describes a sequence of residual stress measurements made to determine a two-dimensional map of biaxial residual stress in a stainless steel weld. A long stainless steel (316L) plate with an eight-pass groove weld (308L filler) was used. The biaxial stress measurements follow a recently developed approach, comprising a combination of contour method and slitting measurements, with a computation to determine the effects of out-of-plane stress on a thin slice. The measured longitudinal stress is highly tensile in the weld and heat affected zone, with a maximum around 450 MPa, and compressive stress toward the transverse edges, around -250 MPa. The total transverse stress has a banded profile in the weld with highly tensile stress at the bottom of the plate (y = 0) of 400 MPa, rapidly changing to compressive stress (at y = 5 mm) of -200 MPa, then tensile stress at the weld root (y = 17 mm) and in the weld around 200 MPa, followed by compressive stress at the top of the weld around -150 MPa. The results of the biaxial map compare well with results of neutron diffraction measurements and output from a computational weld simulation.

Keywords: Residual stress, welding, contour method, computational weld modeling, neutron diffraction, x-ray diffraction

1. INTRODUCTION

The present work is undertaken in the context of understanding weld residual stresses that develop in the fabrication of nuclear power plant piping systems. Welding residual stress is important for nuclear power plant operations because residual stresses can accelerate subcritical failure mechanisms such as stress corrosion cracking [1, 2] or fatigue [3, 4]. For typical piping systems, there are concerns about both axial and circumferential cracks, which requires knowledge of hoop and axial residual stresses. Residual stress data are essential for accurate crack initiation and growth assessment [5]. Furthermore, structural integrity assessment of operating power plants relies upon design codes and procedures [6, 7], that make simplified assumptions regarding the residual stresses present in welds. However, the residual stress field around welds can often be complex, and data for multiple residual stress components are necessary for robust structural integrity assessment [8].

* Corresponding author. Tel.: 530-754-6178; fax: 530-752-4158.
E-mail address: mrhill@ucdavis.edu

Measured biaxial stress fields are also useful for validating computational weld simulation outputs. Weld residual stresses develop as a result of a series of thermomechanical steps, which can be simulated by non-linear finite element computations that provide all the stress components in the weld. But, validation of such computations and estimates of the fidelity of their output requires the measurement of multiple stress components. Such measurements are challenging, and are the subject of on-going research.

Extensive measurement, modeling, and research programs regarding weld residual stress in nuclear power plant piping are underway. One such project has been undertaken cooperatively by the Electric Power Research Institute (EPRI) and the United States Nuclear Regulatory Commission (NRC), working under a memorandum of understanding [9]. The EPRI/NRC weld residual stress program included four phases. Each phase included measurement and modeling of residual stresses, with subsequent phases considering articles of increasing complexity. A summary of program findings are given in [9, 10]. The results show that clear progress has been made in both measuring and modeling of residual stresses in welds, but there is opportunity for improvement. A second large project was organized by the European Network on Neutron Techniques Standardization for Structural Integrity (NeT) [11]. The efforts of the NeT group are ongoing, with several tasks completed, including the characterization of residual stresses from a filled-in slot weld on a plate. The results of this work are given in [12-14] and compare modeling with measurement results, offering advice to improve the fidelity of weld simulation outputs. These programs have shown that biaxial residual stress measurements would be useful.

The simplest way to measure multiple components of residual stress is to choose a measurement technique that directly measures multiple components. Both neutron diffraction and synchrotron x-ray diffraction can form a map of multi-axial residual stress. However, there are several difficulties that arise when making diffraction measurements in prototypical nuclear plant piping geometry. The most problematic is that the structures are usually large (requiring path lengths greater than 25 mm) [9], which significantly increases the time required to make measurements [15]. Also of importance are the microstructural issues present in welds like large grain sizes and texture, that can complicate and cause errors in diffraction measurements [15, 16]. Mechanical stress release methods can be used as an alternative to diffraction methods for welds, since they are insensitive to microstructural issues and can be performed on large parts. One method that inherently measures biaxial residual stress is deep hole drilling [17]. However, deep hole drilling produces measurement data along a line and structural integrity assessments require data on a plane (of anticipated crack growth). Another approach for mapping biaxial stress is to use a superposition of stress release measurements, which is a relatively new approach further considered in this work.

The present work builds on a long history of using mechanical stress release methods to determine multiple components of stress in a weld. Masubuchi has an excellent review of historical residual stress measurement techniques in welded structures [18]. Two mechanical stress release methods were used to find biaxial residual stresses. Gunnert cleverly drilled two sets of small holes through a welded component (one pair set in the longitudinal plane and the other in the transverse plane) and incrementally removed a cylindrical section of the component by cutting an annulus around the holes [19]. Strain found with a specially designed mechanical gage, as the annulus is drilled incrementally, gave data to back calculate residual stress. The modern deep hole drilling method [17] is the descendent of Gunnert's work. Rosenthal and Norton [20] used superposition to determine two components of stress in a weld. They removed two thin slices from a weldment, where the slices came from orthogonal directions (one slice along the longitudinal direction and another along the transverse direction). The

stress release from removing the slices is assumed to vary linearly through plate thickness and is measured using strain gages. Strain gages are mounted on the slice wall and the slices are sectioned into smaller pieces. The strain release during sectioning is used to calculate the stress remaining in the slices. However, both of these methods are time-consuming and prone to relatively large errors [18, 21]. An approach similar to that developed by Rosenthal and Norton (i.e., using superposition) can be employed to measure multiple components of the stress tensor, but with modern measurement techniques enabling better measurement fidelity.

Here we take a preliminary step toward measurements in prototypical nuclear power plant piping systems, and consider a simpler measurement article that allows for development of methodologies to be applied later, in more complex geometries. The present work develops measurements of longitudinal and transverse stress on a cross-section of a long welded plate, using a superposition of multiple mechanical stress release measurements. The measurements include a contour method measurement to determine a two-dimensional map of the longitudinal stress and multiple slitting measurements on a set of removed slices to determine the transverse stress. This methodology assumes the stress release is elastic during each material removal step and that the longitudinal stress does not vary along the weld direction, near a plane of interest.

2. METHODS

The sample used in this study is a long 316L stainless steel plate with an eight-pass groove weld of 308L stainless steel. The plate was the result of a concerted effort to design a sample to obtain data on the precision of residual stress measurements. The plate was designed to have a biaxial weld residual stress field invariant with position along the plate length, except near the ends, while having a stress field representative of the highly constrained welds common in nuclear power plant piping. The plate has a width of 152.4 mm (6 in), height of 25.4 mm (1 in), and a length of 1.22 m (48 in) (Fig. 1a) with a groove along the plate length. The machined groove has a root width of 12.7 mm (0.5 in), root depth of 6.35 mm (0.25 in), and a wall angle of 70º (Fig. 1b). The plate and weld filler metal material properties are given in Table 1. The weld is made with machine controlled inert gas tungsten arc welding (GTAW). The details of the welding procedure can be found elsewhere [22], along with details regarding measured near-weld temperature history, strain history, and weld bead geometry. The coordinate system used in this work has the bottom of the plate at $y = 0$ with positive y upward, the center of the weld at $x = 0$ with positive x to the right (as shown in Fig. 1b). The weld direction, z, is along the plate length, with positive z toward the reader in Fig. 1b and $z = 0$ at the plate mid-length.

Measurement Approach

The measurement process is described with reference to Fig. 2. The part will undergo several machining operations to change its configuration, where each configuration will be identified by a capital letter (i.e., A, B, C). The purpose of this work is to measure the biaxial stress at a longitudinal plane at the center of the long welded plate (configuration A), which is indicated as the hatched plane in Fig. 2. All components of the stress tensor, at the plane of interest in configuration A, will be identified as σ^A. Two other configurations are also used: one after the part is cut in half (configuration B), and one after a thin slice is removed adjacent to the plane of interest (configuration C).

During each configuration change, residual stresses are released, and released stress is defined as the change in stress between the current configuration and the prior configuration, denoted with an italic roman numeral. Fig. 2 shows all configuration changes and their associated stress release (e.g., $\sigma^{i} = \sigma^{A} - \sigma^{B}$ and $\sigma^{ii} = \sigma^{B} - \sigma^{C}$). With superposition, σ^A can be found as

$$\sigma^A = \sigma^i + \sigma^{ii} + \sigma^C. \quad (1)$$

The stress release between configurations A and B (σ^i) is found using the contour method. The stress remaining in the slice (σ^C) will be found with slitting (only transverse stress, since longitudinal stress in the thin slice is assumed to be zero). Previous work has shown that stress in parts with locally smooth stress relative to out-of-plane position (e.g., along the length of the plate) can be decomposed into two distinct stress states, the stress remaining in the thin slice, and the effect of the longitudinal stress on a thin slice, as illustrated in Fig. 3. A numerical verification of the stress decomposition has been shown in [23], and an experimental validation in [24]. This stress decomposition gives

$$\sigma^A = \sigma^{A(z)} + \sigma^C \quad (2)$$

where $\sigma^{A(z)}$ is the effect of the longitudinal stress on the thin slice. The prior work [23, 24] also shows that $\sigma^{A(z)}$ can be fully determined from σ^i, which allows σ^A to be determined without measuring σ^{ii}.

The stress change σ^i was found using the contour method, which was established by Prime [25]. He showed that when a part containing residual stress is cut in half, deformations are caused by the release of residual stress. The released residual stress can be found by measuring the out-of-plane displacements on the cut surface and finding the stress required to return the cut surface to its original planar configuration, which can be accomplished using an elastic finite element analysis. The experimental steps of the contour method and its application to the present long welded plate are described in a companion paper [22]; the measurement used here was identified in the earlier work as Cut 1. The plate was cut at an intersecting plane at the mid-length ($z = 0$) using a wire electric discharge machine (EDM), while securely clamped. The two resulting deformed cut surfaces were measured with a laser scanning profilometer along the cross-section with a measurement spacing of 100 μm in the vertical direction and 200 μm in the horizontal direction, so that there were roughly 190,000 data points for each surface. The two surface profiles were then averaged on a common grid, and the average was fit to a smooth bivariate analytical surface. Residual stress on the contour plane was found by applying the negative of the smoothed surface profile as a displacement boundary condition in a linearly elastic finite element (FE) model of the half plate. The FE analysis used commercial software [26], and a mesh of eight-node linear interpolation brick elements, with node spacing of 1 mm on the cross-section in both directions, and biased node spacing in the out-of-plane direction, being 1 mm at the contour cut plane and 4 mm at the free end. The total number of finite elements was 180,000. The elastic modulus and Poisson's ratio were assumed to be 206 GPa and 0.3 for both the parent metal and the filler weld material, since there is little difference between the two as is shown in Table 1.

Stress in the slice, σ^C, along the transverse direction was found with several slitting measurements on four slices, to form a map of transverse stress (Fig. 5). The slices had a thickness of 6.35 mm (0.25 in) and were removed at z = -6.35, -12.7, 6.35, and 12.7 mm for slice 1 through 4, respectively. Measurements were made by cutting along the yz plane starting from the top of the slice at x = -12.7, 0, and 12.7 mm for slices 1 and 3 and at x = -19.05, -6.35, 6.35, and 19.05 mm for slices 2 and 4. A diagram of the all the sectioning steps is shown in Fig. 4 to more easily understand the configuration changes. The plate is assumed to have constant stress along its length, so slitting measurements on different slices are collapsed onto a single measurement plane. Slitting measurements consist of cutting a slit into the material with a wire EDM in several depth increments, while measuring strain at the back face of the cut plane for each cut increment, where the back face in these samples is the bottom of the plate near $y = 0$. Stress is then calculated from strain versus cut depth data using an elastic inverse [27], with Tikhonov regularization to smooth the stress by penalizing its second derivative [28]. The

correction scheme by Aydiner and Prime [29] was used to accurately reflect the finite thickness of the slice by slightly altering a stress analysis that was based upon a plane strain finite element model.

Each slitting measurement introduces a new stress-free surface, which will redistribute the stress in the body. Of course, the stress redistribution is more significant near the new free surface and less significant away from that surface. So when performing mapping using multiple slitting measurements, it is necessary to find the effect of a prior slitting measurement on a subsequent measurement. The procedure is to apply the stress measured in the prior slitting measurement as a traction boundary condition within a finite element model of the specimen after the prior measurement (i.e. apply the measured stress at the measurement plane from the prior measurement) and extract the resulting stress at the subsequent measurement plane. We refer to the stress at a given measurement plane, due to cutting at a prior plane as a "correction". The stress correction approach for adjacent slitting measurements has been validated in prior work [30, 31].

The effect of the longitudinal stress on the in-plane stress components in a thin slice, $\sigma^{A(z)}$, was found using an elastic finite element simulation. The model has the same geometry as the slices in the slitting measurements, but assumes half-thickness symmetry. The longitudinal stress determined by the contour method is applied as a traction boundary condition on the face of the slice, and the resulting in-plane stress provides the unknown $\sigma^{A(z)}$. The analysis used a mesh with node spacing of 0.75 mm by 0.75 mm in the in-plane directions and eight elements across the thickness, with a total of roughly 64,500 eight-node linear brick elements with incompatible modes (ABAQUS element type C3D8I), which allows linearly varying pressure across the element. The material was assumed to be linear elastic with properties stated earlier.

Uncertainty

An uncertainty analysis is useful in multi-step measurements so that sources of error can be accounted for, and minimized where possible. The uncertainty of the contour method was found using the methodology developed in [32]. The two principal error sources in contour measurements are the error associated with noise in the displacement data (due to surface roughness inherent in EDM cuts and errors in measurement of the surface profile), called the displacement error, and the error associated with smoothing the surface displacement, called the model error. The displacement error is found by repeatedly (5x) applying normally distributed noise to the surface profile, then taking the standard deviation of the five resulting stress distributions. The model error is found by taking the standard deviation of the resulting stresses from different, "nearby", levels of smoothing. The total uncertainty in the weld direction stress, $\sigma_{zz}(x, y)$ is found by taking the two error sources in quadrature

$$U_{zz,tot} = \sqrt{U_{zz,disp}^2 + U_{zz,model}^2} \tag{3}$$

where $U_{zz,tot}$ is the total uncertainty (in the longitudinal stress), $U_{zz,disp}$ is the displacement error, and $U_{zz,model}$ is the model error.

The uncertainty associated with the slitting measurements was computed using the procedure given in [33]. Since regularized unit pulses were used as the basis functions, the model error term was excluded and only the random uncertainty term was taken as the maximum of the misfit between measured strain and fit strain, or a minimum value of 2 με.

The uncertainty in $\sigma^{A(z)}$ was found using a Monte Carlo approach. The uncertainty was estimated by taking the standard deviation of the results of $\sigma^{A(z)}$ when the underlying longitudinal stress had normally distributed noise with a standard deviation corresponding to the uncertainty in the longitudinal stress. The two uncertainty sources for the transverse stress are combined in quadrature

$$U_{xx,tot} = \sqrt{U_{xx,C}^2 + U_{xx,A(z)}^2} \tag{4}$$

where $U_{xx,tot}$ is the total uncertainty (in the transverse stress), $U_{xx,C}$ is the uncertainty in the transverse stress remaining in the slice, and $U_{xx,A(z)}$ is the uncertainty in the effect of the longitudinal stress on the thin slice.

Comparison Data

Since the biaxial stress mapping approach is new, comparison stress data were developed using a complementary experimental method and a weld simulation. Neutron diffraction measurements were made on a 152.4 mm (6 in) long section of the plate, and employed the standard methodologies for neutron diffraction measurements described in [34]. Lattice spacing (d-spacing) was measured in three orthogonal directions at a set of in-plane locations at the sample mid-length, and at an identical set of in-plane locations in a stress-free sample (d_0-spacing) that was cut free from the weld, as described below. The neutron diffraction measurements were made at SMARTS [35], a time-of-flight instrument with two detector banks at ±90º from the incident neutron beam, which allows two orthogonal lattice spacings to be measured simultaneously. However, due to the large thickness of the plate, it proved that for most of the measurement locations, only one component of the lattice spacing could be measured at a time. The lattice spacings were found using the full diffraction pattern with GSAS [36]. The normal residual strain components were found using

$$\varepsilon_i = \frac{d_i - d_{i,0}}{d_{i,0}} \tag{5}$$

where ε_i is strain and i denotes the transverse, through-thickness, or weld direction strain component and corresponding lattice spacing. The residual stresses were calculated using Hooke's Law

$$\sigma_i = \frac{E}{(1+\nu)(1-2\nu)}\left[(1+\nu)\varepsilon_i + \nu\left(\varepsilon_j + \varepsilon_k\right)\right] \tag{6}$$

where σ_i is a stress component, E is the elastic modulus, and ν is Poisson's ratio, and where the subscript i refers to a stress component of interest (xx, yy, or zz) and the corresponding strain, and where j and k refer to the other two strain components.

The sample used to measure stress free lattice spacing, d_0, at different locations in the weld was made by cutting a "waffle" pattern 10 mm into the end of a small (15 mm) length of the welded plate (Fig. 6). A d_0 sample with this geometry has the advantage that there is a high degree of confidence that the measurement locations will be the same between the d and d_0 samples, since the "teeth" in the d_0 waffle pattern have very small deflections from the positions before cutting (the fully intact back portion of the plate keeps the sample rigid). However, with this type of d_0 sample, the added thickness increases the measurement time by a roughly a factor of 9, because count time is related to the square of thickness (sample is 3 times thicker than more typical stress-free cubes).

A finite element welding simulation has been performed for this plate, to provide residual stress output for comparison with the measured stress. The model assumed a representative 152.4 mm (6 in) long geometry, and the simulation consisted of two sequentially-coupled analysis steps, the first thermal and the second mechanical, conducted in commercial finite element software [26]. The three-dimensional mesh contained 24,912 finite elements, where 20-node quadratic heat transfer bricks (DC3D20) were used in the thermal analysis and 20 node reduced integration quadratic bricks (C3D20R) were used in the mechanical analysis. The node spacing was small near the weld (around 1 mm) and larger away from the weld. Both the plate and filler weld metal used the temperature-dependent thermo-physical and thermo-mechanical material properties of 316L given in [37]. The thermal analysis used an ellipsoidal volumetric heat source that was calibrated using a welding heat source modeling tool [38] and near-weld temperature history data that was collected during plate fabrication. The resulting temperature field for each pass that was calculated in the thermal analysis was used as input for the subsequent mechanical analysis. The mechanical analysis used the mixed isotropic-kinematic work hardening model for 316L found in [37]. The mechanical analysis used a Lagrangian mesh with a small strain model, since there wasn't a need for large deformations to be considered (and was shown by the good convergence of the model). Further details on the simulation can be found in a related paper [39, 40].

3. RESULTS

Fundamental measurement data for the contour method comprises the two surface profiles, the average of the two surface profiles, and the smoothed (fit) profile. Line plots from the two-dimensional surface data are shown in Fig. 7, taken from a 0.1 mm band around $y = 17$ mm along the horizontal direction and $x = 0$ along the vertical direction. The surface profiles have similar shapes, which indicates the clamping was of good quality, and provided the same level of support to each half of the part as it was being cut. The smoothed profile shows the chosen fit appropriately removes noise without altering the underlying form.

Residual stress from the contour measurement can be seen in Fig. 8a. There is high tensile stress in the weld and heat affected zone, with a maximum of 450 MPa giving way to compression away from the weld. The longitudinal stress from the computational weld model can be seen in Fig. 8b. The computational weld model has very good agreement with the measured stress near the weld root, but the two have some level of disagreement toward the top of the weld and also far from the weld, toward the transverse edges.

The measured strain and stress from the slitting measurement on slice 3 at $x = 0$ can be seen in Fig. 9, which are typical of other slitting measurements. Results from all slitting measurements are shown in Fig. 10, where the lines represent the average of the two measurements (on different slices) at each location, and the full error bar represents the range between the two measurements. Measured stresses are consistent between slices, as shown by small error bars (10 to 20 MPa) at most locations, but with some locations having significant differences, with particularly large error bars near a sharp stress gradient evident at the bottom of the plate near the weld center.

The average slitting measurements are plotted as a map of transverse stress in the slice (σ^{C}) in Fig. 11, which also shows the effect of the longitudinal stress on transverse stress ($\sigma^{A(z)}$), and the total transverse stress (σ^{A}). The transverse stress in the slice (Fig. 11a) shows bands of stress along the width of the plate with highly tensile stress at the bottom of the plate around 400 MPa, then compressive stress at $y = 5$ mm around -200 MPa, then tensile stress at the weld root ($y = 17$ mm) around 200 MPa,

followed by compressive stress at the top of the weld around -100 MPa. The effect of the longitudinal stress on the thin slice (Fig. 11b) has low magnitude in compression around -30 MPa from the bottom of the plate to y = 10 mm, then tensile stresses around 50 MPa from y = 12 to 22 mm, then turns sharply negative near the weld crown to around -100 MPa. The total transverse stress (Fig. 11c) has a trend similar to the stress remaining in the slice, but significantly lower in the weld, around -150 MPa. A line plot showing the contributions to the total transverse stress is shown in Fig. 12, which illustrates that $\sigma^{A(z)}$ is a minor, but needed, contributor to the total transverse stress. The transverse stress from the computational weld model in Fig. 11d has a distribution in the weld center similar to the measurements, but with somewhat smaller magnitude.

The uncertainties in measured residual stress are shown in Fig. 13 and Fig. 14. The uncertainty in longitudinal stress is highest near the transverse edges of the plate and at the top of the weld (over 50 MPa), but is under 30 MPa for a large portion of the interior cross-section. For the transverse stress, the uncertainty from the stress remaining in the slice is very small, with a high of 8 MPa near the bottom of the plate. The uncertainty in the slitting measurements is excellent and agrees with previous studies [41]. The uncertainty due to the effect of the longitudinal stress is somewhat high near the transverse edges of the plate and at the top of the weld (both over 20 MPa), but is under 10 MPa for a large portion of the interior cross-section. The total uncertainty has a distribution that is dominated by the uncertainty due to the effect of the longitudinal stress and has essentially the same distribution.

Line plots for the longitudinal stress from biaxial mapping using mechanical stress release methods (mechanical), neutron diffraction (ND), and computational weld modeling (FE) can be seen in Fig. 15. The results along y = 17 mm agree very well around the weld. Differences away from the weld are thought to be caused by the presence of tack welds in the manufacturing of the plate, discussed at length in [22]. Along the vertical direction at the weld center, the longitudinal stresses from the mechanical approach and the FE computation also agree fairly well. The major difference is at the top of the weld. The neutron diffraction results show a similar trend of low level tension below the weld (y = 0 to 10 mm) and high tension in the weld, where the neutron diffraction result at y = 22.5 mm (Fig. 15b) is an outlier.

Line plots of the transverse stress from the three methods can be seen in Fig. 16 and shows reasonable agreement between all three methods. For the line plot traversing the x-direction at y = 17 mm (Fig. 16a), there is excellent agreement between the mechanical mapping and the weld model, and reasonable agreement with the neutron diffraction results, except at x = 0 where the neutron result is an outlier. For the line plot traversing the y-direction at weld center (Fig. 16b), there is good agreement between the mechanical biaxial mapping and the weld model in the weld (y > 12 mm), but a significant difference at the bottom of the plate where the measured stress transitions very quickly from compression (-200 MPa at y = 5 mm) to high tension (400 MPa at y = 2 mm). The neutron diffraction results agree fairly well with the other techniques along the weld center, but with results at y = 17.5 and 22.5 mm being outliers. To further investigate the discrepancy in transverse stress near the back face, follow-on x-ray measurements were performed, as described below.

4. DISCUSSION

The weld residual stress measured with mechanical biaxial mapping is typical of a well-restrained weld, with weld direction stress having high tension in the weld metal and heat-affected zone, and compression away from the weld. The transverse weld residual stress is tensile, with the maximum below the surface, which is typical of restrained welds [42]. The results of the mechanical biaxial

mapping have reasonable agreement with the complementary measurements and output from the weld simulation. Although the fundamental mechanics of the mechanical biaxial mapping approach have been validated numerically [23], the good agreement here instills further confidence in the new approach.

The high tensile transverse stress at the bottom of the plate found with mechanical biaxial mapping was not predicted by the computational weld model. To further investigate transverse stress near the back face, additional x-ray diffraction measurements were made in a removed slice identical to the slices used for slitting measurements. Measurements were made on the face of the slice at the weld center ($x = 0$) and at $y = 1$, 2, 3, and 4 mm. Electropolish was used to remove the effects of the EDM cuts used to create the slice. The measurement used a two-angle $\sin^2\psi$ technique and the 311 *hkl* plane. The measurement rotated ψ between 10º and 50º. The sample was rocked through an angular range of ±1.5º around the mean ψ angles during measurement to integrate the diffracted intensity over more grains in order to minimize the influence of the grain size. The value of the x-ray elastic constant was assumed to be 183 GPa. To allow comparison of the x-ray data with the transverse stress in the original plate, $\sigma^{A(z)}$ was added to the x-ray results, which amounts to a small correction (at the weld center, $\sigma^{A(z)}$ varies from 0 MPa at $y = 0$ to 40 MPa at $y = 4$ mm (Fig. 12)). The measured transverse stress from the mechanical biaxial mapping, neutron diffraction, and x-ray diffraction are nominally consistent, as shown in Fig. 16. This suggests that the FE model might not be capturing some local conditions at the plate back face that were present during welding, which resulted in a localized model discrepancy.

The neutron diffraction measurements in this plate were difficult. The diffraction patterns found had very little signal relative to the background noise, due to the large thickness of the plate. As can be seen in a typical set of data for one location (Fig. 17), the diffraction pattern has small peaks relative to background noise. Because the stresses in the plate are expected to be symmetric about the weld centerline, the d and d_0-spacings were averaged at points at equal distance from the weld center and at the same vertical location. Further, two components of d_0 (longitudinal and transverse) were also averaged, since the material has a cubic crystalline lattice and the two stress-free spacings should be equal. Both of these data processing steps reduced noise in the neutron diffraction results. To give a better idea of the spread in the data, the uncertainty was found by taking the standard deviation of the stresses that were equal distance from the weld centerline without averaging the d and d_0 measurements. For the measurements along the weld center-line, uncertainty was estimated using standard error propagation [43], where the misfit in lattice spacing given from the Rietveld refinement using GSAS was the underlying uncertainty. The neutron diffraction uncertainties can be seen as error bars in the line plots in Fig. 15 and Fig. 16.

5. SUMMARY/CONCLUSIONS

A biaxial mapping methodology using mechanical stress release methods was applied to measure residual stress in a long welded rectangular plate. The measurement consisted of decomposing the initial residual stresses into the longitudinal stress, stress remaining in a thin slice, and the effect of the longitudinal stress on a slice. The longitudinal stress is found using the contour method. The effect of the longitudinal stress on a thin slice is found with a linear elastic stress analysis. The transverse stress remaining in the slice is found using several slitting measurements.

The longitudinal stress is highly tensile in the weld and heat affected zone, with a maximum around 450 MPa and compressive away from the weld. The total transverse stress has a banded profile with highly tensile stress at the bottom of the plate around 400 MPa, then compressive stress at $y = 5$ mm

around -200 MPa, then tensile stress at the weld root (y = 17 mm) around 200 MPa, followed by compressive stress at the top of the weld around -150 MPa.

The results of the biaxial mapping measurement were compared to neutron diffraction measurements, x-ray diffraction measurements, and the results of a computational weld simulation. The results agree well overall, but there are some differences. The differences with the weld model might result from not capturing the all the details of the boundary conditions present during fabrication, such as an interaction with the I-beam during welding.

The results of this work show that biaxial residual stress can be effectively measured in a relatively simple geometry with a stress field that is representative of a highly constrained weld. The new mechanical biaxial mapping approach is applicable to large and complex weldments, as demonstrated in [44], and may prove a promising tool for use in structural integrity evaluation of nuclear power plant components.

6. ACKNOWLEDGEMENTS

With gratitude, the authors acknowledge Eric Willis, Artie Peterson, and Mike Newman of EPRI Welding and Repair Technology Center (WRTC) for fabricating the plate used in this study. The Electric Power Research Institute, Materials Reliability Program (Paul Crooker, Principal Technical Leader) provided financial support for this work.

REFERENCES

[1] EPRI, "Material Reliability Program Crack Growth Rates for Evaluating Primary Water Stress Corrosion Cracking (PWSCC) of Alloy 82, 182, and 132 Welds", MRP-115NP, Electric Power Research Institute, 2004.

[2] F. W. Brust and P. M. Scott, "Weld residual stresses and primary water stress corrosion cracking in bimetal nuclear pipe welds", PVP2007-26297, ASME 2007 Pressure Vessels and Piping Conference, 2007.

[3] T.-K. Song, H.-R. Bae, Y.-J. Kim, and K.-S. Lee, "Numerical investigation on welding residual stresses in a PWR pressurizer safety/relief nozzle", *Fatigue & Fracture of Engineering Materials & Structures,* vol. 33, pp. 689-702, 2010.

[4] M. N. James, D. J. Hughes, Z. Chen, H. Lombard, D. G. Hattingh, D. Asquith*, et al.*, "Residual stresses and fatigue performance", *Engineering Failure Analysis,* vol. 14, pp. 384-395, 2007.

[5] M. Kerr, M. B. Prime, H. Swenson, M. A. Buechler, M. Steinzig, B. Clausen*, et al.*, "Residual Stress Characterization in a Dissimilar Metal Weld Nuclear Reactor Piping System Mock Up", *Journal of Pressure Vessel Technology,* vol. 135, p. 041205, 2013.

[6] ASME, "Boiler and Pressure Vessel Code", American Society of Mechanical Engineers, New York, USA, 2013

[7] British Energy Generation Ltd, "Procedure R6 Revision 4: Assessment of the integrity of structures containing defects", Gloucester, UK, 2004

[8] L. Edwards, M. C. Smith, M. Turski, M. E. Fitzpatrick, and P. J. Bouchard, "Advances in residual stress modeling and measurement for the structural integrity assessment of welded thermal power plant", *Advanced Materials Research,* vol. 41, pp. 391-400, 2008.

[9] EPRI, "Materials Reliability Program: Finite-Element Model Validation for Dissimilar Metal Butt-Welds", MRP-316, Electric Power Research Institute, 2011.

[10] H. J. Rathbun, L. F. Fredette, P. M. Scott, A. A. Csontos, and D. L. Rudland, "NRC Welding Residual Stress Validation Program International Round Robin Program and Findings", PVP2011-57642, 2011 ASME Pressure Vessels & Piping Division Conference, Baltimore, MD, USA, 2011.

[11] C. Truman and M. Smith, "The NeT residual stress measurement and modelling round robin on a single weld bead-on-plate specimen", *International Journal of Pressure Vessels and Piping,* vol. 86, pp. 1-2, 2009.

[12] C. Ohms, R. C. Wimpory, D. E. Katsareas, and A. G. Youtsos, "NET TG1: Residual stress assessment by neutron diffraction and finite element modeling on a single bead weld on a steel plate", *International Journal of Pressure Vessels and Piping,* vol. 86, pp. 63-72, 2009.

[13] M. C. Smith and A. C. Smith, "NeT bead-on-plate round robin: Comparison of residual stress predictions and measurements", *International Journal of Pressure Vessels and Piping,* vol. 86, pp. 79-95, 2009.

[14] P. J. Bouchard, "The NeT bead-on-plate benchmark for weld residual stress simulation", *International Journal of Pressure Vessels and Piping,* vol. 86, pp. 31-42, 2009.

[15] M. T. Hutchings, P. J. Withers, T. M. Holden, and T. Lorentzen, "*Introduction to the Characterization of Residual Stress by Neutron Diffraction*", Boca Raton, FL, CRC Press, 2005.

[16] W. Woo, H. Choo, M. Prime, Z. Feng, and B. Clausen, "Microstructure, texture and residual stress in a friction-stir-processed AZ31B magnesium alloy", *Acta materialia,* vol. 56, pp. 1701-1711, 2008.

[17] D. J. Smith, *Practical Residual Stress Measurement Methods*, Ch. 3, John Wiley & Sons, West Sussex, UK, 2013

[18] K. Masubuchi, *Analysis of welded structures: Residual stresses, distortion, and their consequences*, Ch. 4, Pergamon Press, New York, NY, 1980

[19] R. Gunnert, *Proceedings of the Special Symposium on the Behavior of Welded Structures*, Ch. University of Illinois, 1961

[20] D. Rosenthal and J. Norton, "A method of measuring triaxial residual stress in plates", *Welding Journal,* vol. 24, pp. 295s-307s, 1945.

[21] M. R. Hill and D. V. Nelson, "Determining residual stress through the thickness of a welded plate", *ASME-PUBLICATIONS-PVP,* vol. 327, pp. 29-36, 1996.

[22] M. D. Olson, M. R. Hill, E. Willis, A. G. Peterson, V. I. Patel, and O. Muránsky, "Assessment of Weld Residual Stress Measurement Precision: Mock-Up Design and Results for the Contour Method", *Journal of Nuclear Engineering and Radiation Science,* 2014.

[23] M. D. Olson, W. Wong, and M. R. Hill, "Simulation of Triaxial Residual Stress Mapping for a Hollow Cylinder", PVP2012-78885, ASME 2012 Pressure Vessels & Piping Conference, Toronto, Ontario, Canada, 2012.

[24] M. D. Olson and M. R. Hill, "Biaxial Residual Stress Mapping Validation", *Submitted for publication in Experimental Mechanics,* 2014.

[25] M. B. Prime and A. R. Gonzales, "The Contour Method: Simple 2-D Mapping of Residual Stresses", Sixth International Conference on Residual Stresses, Oxford, UK, 2000.

[26] Abaqus/Standard, Version 6.10, Providence, RI, USA, 2010.

[27] M. R. Hill, *Practical Residual Stress Measurement Methods*, Ch. 4, John Wiley & Sons, West Sussex, UK, 2013

[28] G. S. Schajer and M. B. Prime, "Use of Inverse Solutions for Residual Stress Measurement", *Journal of Engineering Materials and Technology,* vol. 128, pp. 375-382, 2006.

[29] C. C. Aydıner and M. B. Prime, "Three-dimensional constraint effects on the slitting method for measuring residual stress", *Journal of Engineering Materials and Technology,* vol. 135, 2013.

[30] M. D. Olson and M. R. Hill, "Residual Stress Mapping with Slitting", *Manuscript in preparation for publication in Experimental Mechanics,* 2014.

[31] W. Wong and M. R. Hill, "Superposition and Destructive Residual Stress Measurements", *Experimental Mechanics,* vol. 53, pp. 339-344, 2013.

[32] M. D. Olson, A. T. DeWald, M. R. Hill, and M. B. Prime, "Contour Method Uncertainty Estimation", *Experimental Mechanics,* 2014.

[33] M. B. Prime and M. R. Hill, "Uncertainty, Model Error, and Order Selection for Series-Expanded, Residual-Stress Inverse Solutions", *Journal of Engineering Materials and Technology,* vol. 128, p. 175, 2006.

[34] ISO, "Non-destructive testing - Standard test method for determining residual stresses by neutron diffraction", ISO/TS 21432, International Organization for Standardization, 2005.

[35] M. A. M. Bourke, D. C. Dunand, and E. Ustundag, "SMARTS - a spectrometer for strain measurement in engineering materials", *Applied Physics A: Materials Science & Processing,* vol. 74, pp. s1707-s1709, 2002.

[36] A. C. Larson and R. B. Von Dreele, "General Structural Analysis System (GSAS)", *Los Alamos National Laboratory Report LAUR 86-748,* 2004.

[37] O. Muránsky, M. Smith, P. Bendeich, T. Holden, V. Luzin, R. Martins*, et al.*, "Comprehensive numerical analysis of a three-pass bead-in-slot weld and its critical validation using neutron and

synchrotron diffraction residual stress measurements", *International Journal of Solids and Structures,* vol. 49, pp. 1045-1062, 2012.

[38] FeatPlus, FEAT-Weld Modeling Tools, Version 2.0, Bristol, UK, 2010.

[39] V. I. Patel, O. Muránsky, C. J. Hamelin, M. D. Olson, M. R. Hill, and L. Edwards, "A Validated Numerical Model for Residual Stress Predictions in an Eight-Pass-Welded Stainless Steel Plate", Materials Science Forum, 2013.

[40] V. I. Patel, O. Muránsky, C. J. Hamelin, M. D. Olson, M. R. Hill, and L. Edwards, "Finite Element Modelling Of Welded Austenitic Stainless Steel Plate With 8-Passes", PVP2014-28209, ASME 2014 Pressure Vessels & Piping Division Conference, Anaheim, CA, USA, 2014.

[41] M. J. Lee and M. R. Hill, "Intralaboratory Repeatability of Residual Stress Determined by the Slitting Method", *Experimental Mechanics,* vol. 47, pp. 745-752, 2007.

[42] J. Zhang and P. Dong, "Residual stresses in welded moment frames and implications for structural performance", *Journal of Structural Engineering,* vol. 126, pp. 306-315, 2000.

[43] H. W. Coleman and W. G. Steele, *Experimentation, Validation, and Uncertainty Analysis for Engineers*, Ch. 2, John Wiley & Sons, Inc., Hoboken, New Jersey, 2009

[44] M. R. Hill, M. D. Olson, and A. T. DeWald, "Biaxial Residual Stress Mapping for a Dissimilar Metal Welded Nozzle", PVP2014-28328, ASME 2014 Pressure Vessels & Piping Division Conference, Anaheim, CA, USA, 2014.

TABLES

Material	E (GPa)	ν	Yield Strength (MPa)
316L Stainless steel	206	0.30	440
308L Stainless steel	204	0.30	350

Table 1: Material properties

FIGURES

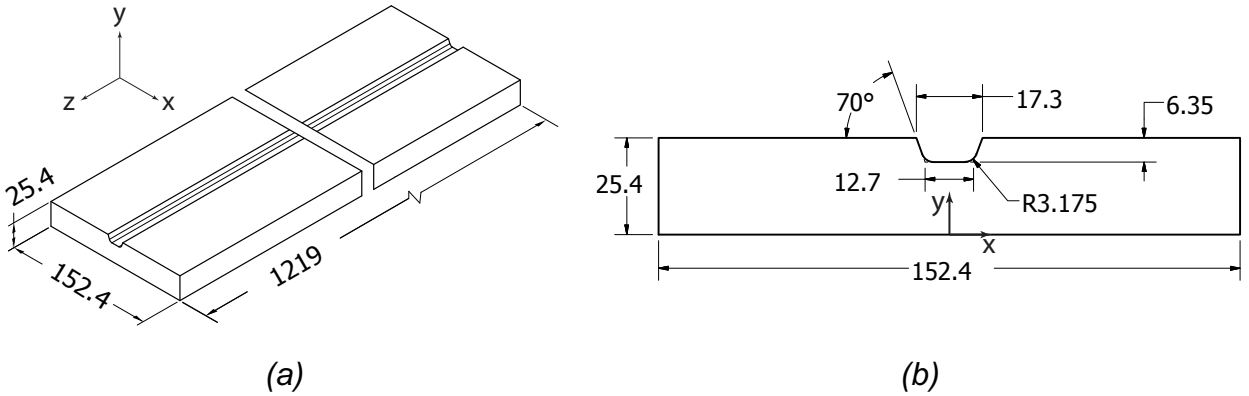

Fig. 1 – Dimensioned diagram of the plate (a) overall geometry and (b) cross-section with details of the machined groove. All dimensions are in mm

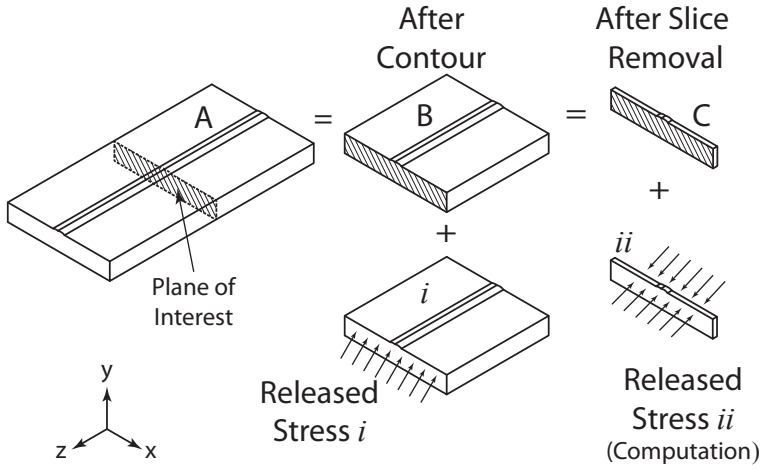

Fig. 2 – Experimental step diagram. The initial configuration (A) is cut in half to the B configuration and the stress release σ^{i} is found with the contour method. A slice (configuration C) is then removed from the B configuration. The stress release σ^{ii} is not directly found, but could be found as $\sigma^{ii} = \sigma^{A} - \sigma^{C} - \sigma^{i} = \sigma^{A(z)} - \sigma^{i}$. Plane of interest (z=0) is shown as a hatched plane

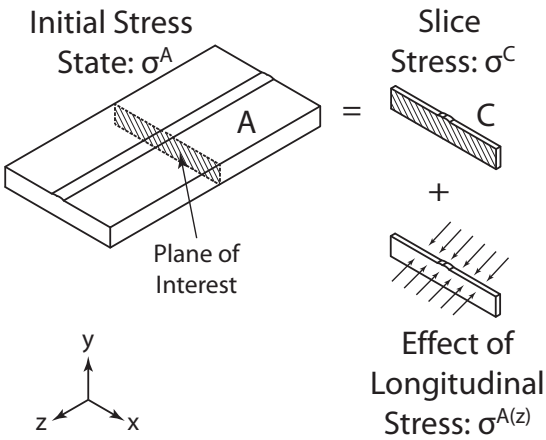

Fig. 3 – Stress decomposition diagram. The original stress (σ^A) is equal to the stress remaining in a thin slice (σ^C) plus the effect of total longitudinal stress on the thin slice ($\sigma^{A(z)}$). Plane of interest (z=0) is shown as a hatched plane

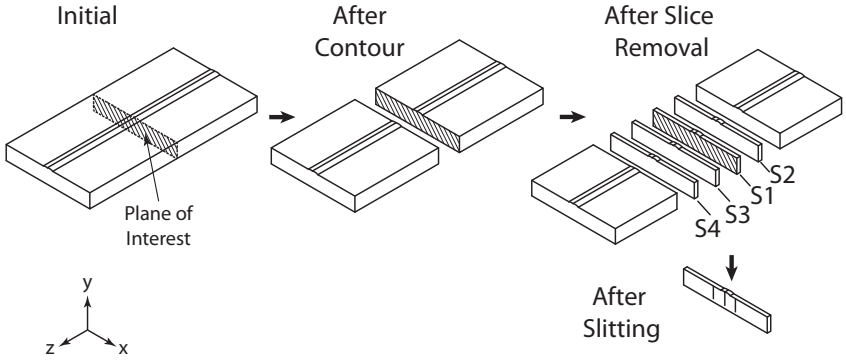

Fig. 4 – The sectioning steps used the in the biaxial mapping experiment. Plane of interest (z=0) is shown as a hatched plane

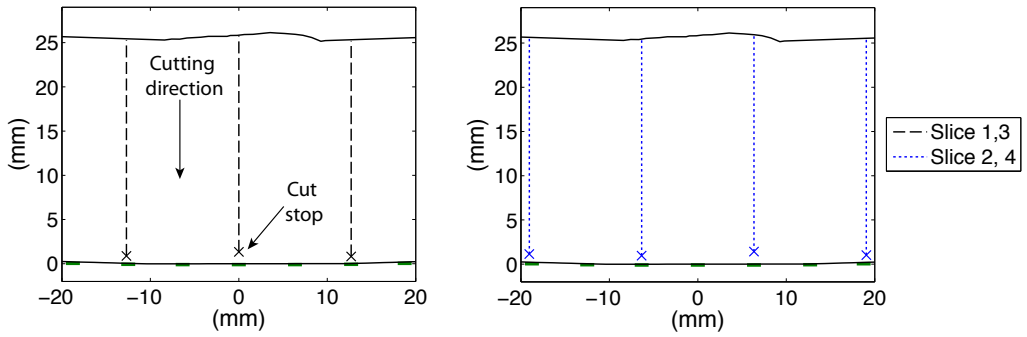

Fig. 5 – Slitting plane locations to determine remaining transverse stresses in the slice. Repeat measurements were made for the slices 1, 3 and for slices 2, 4. Strain gages (to scale) are shown as thick lines on bottom of slice. The slitting direction is from the top of the figure to the bottom and the maximum cut depth is indicated with an x

Fig. 6 – Neutron diffraction stress-free (d_0) sample

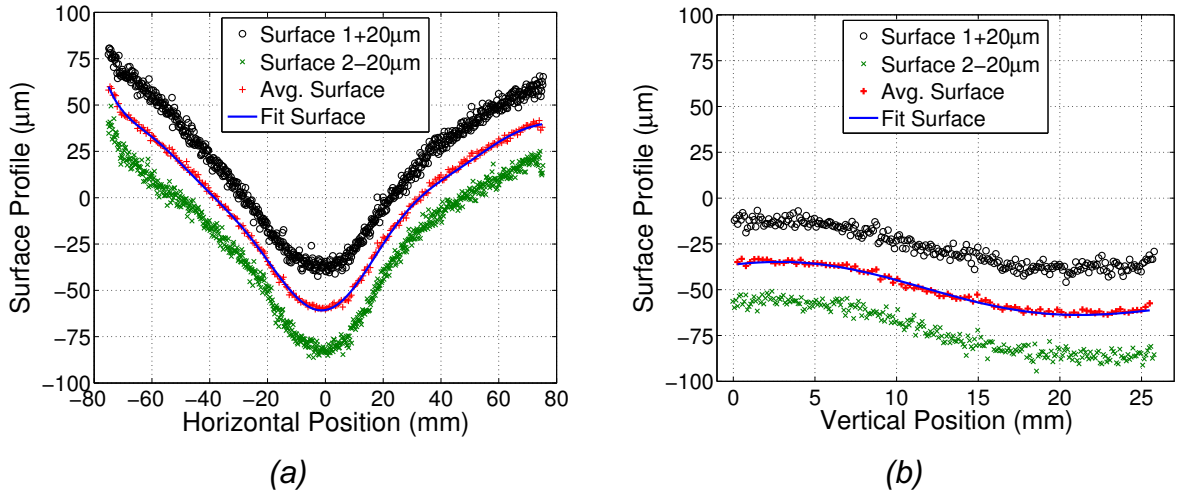

Fig. 7 – Line plots of the surface displacements (20 μm added to surface 1 and 20 μm subtracted from surface 2), average surface, and fit surface from the contour measurement (a) horizontal direction at y = 17 mm and (b) along the vertical at the weld center (x = 0)

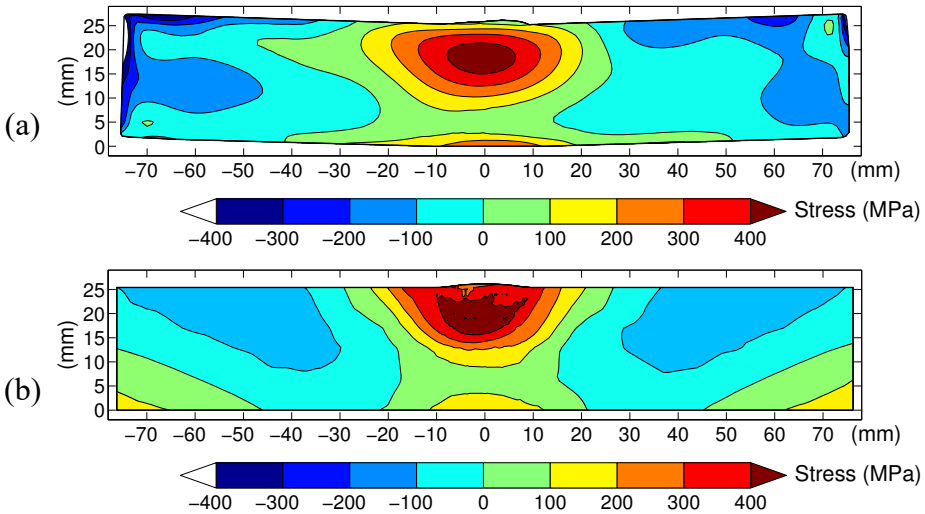

Fig. 8 – (a) Measured longitudinal stress using the contour method and (b) longitudinal stress from a computational weld model

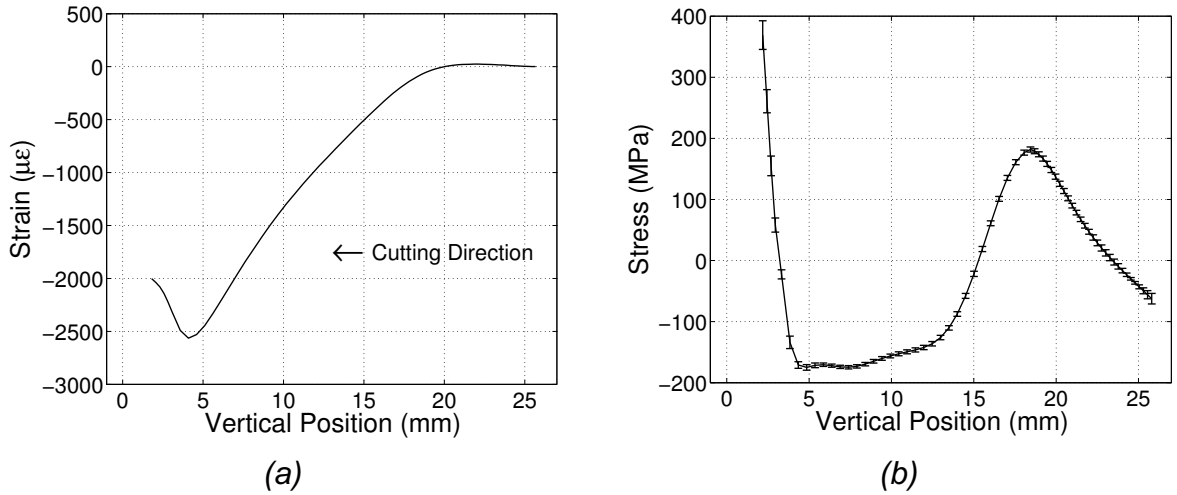

Fig. 9 – Slitting data at x = 0 on slice 3 (a) measured strain and (b) the computed stress

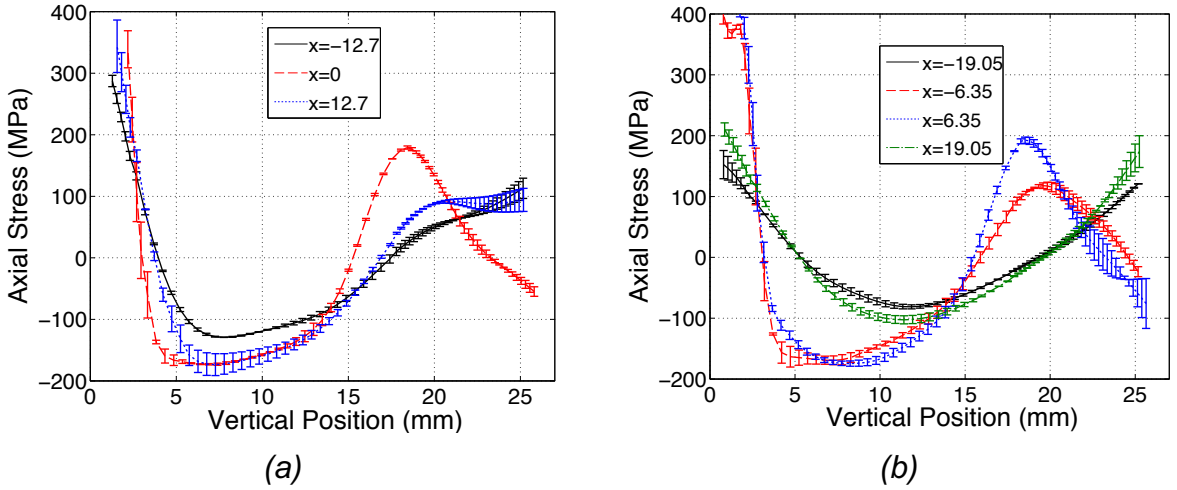

Fig. 10 – Average of the slitting data for where the line is the average and the error bars are half the range (so that the top of the error bar touches one measurement and the bottom of the error bar touches the other measurement) for (a) slices 1 and 3, and (b) slices 2 and 4

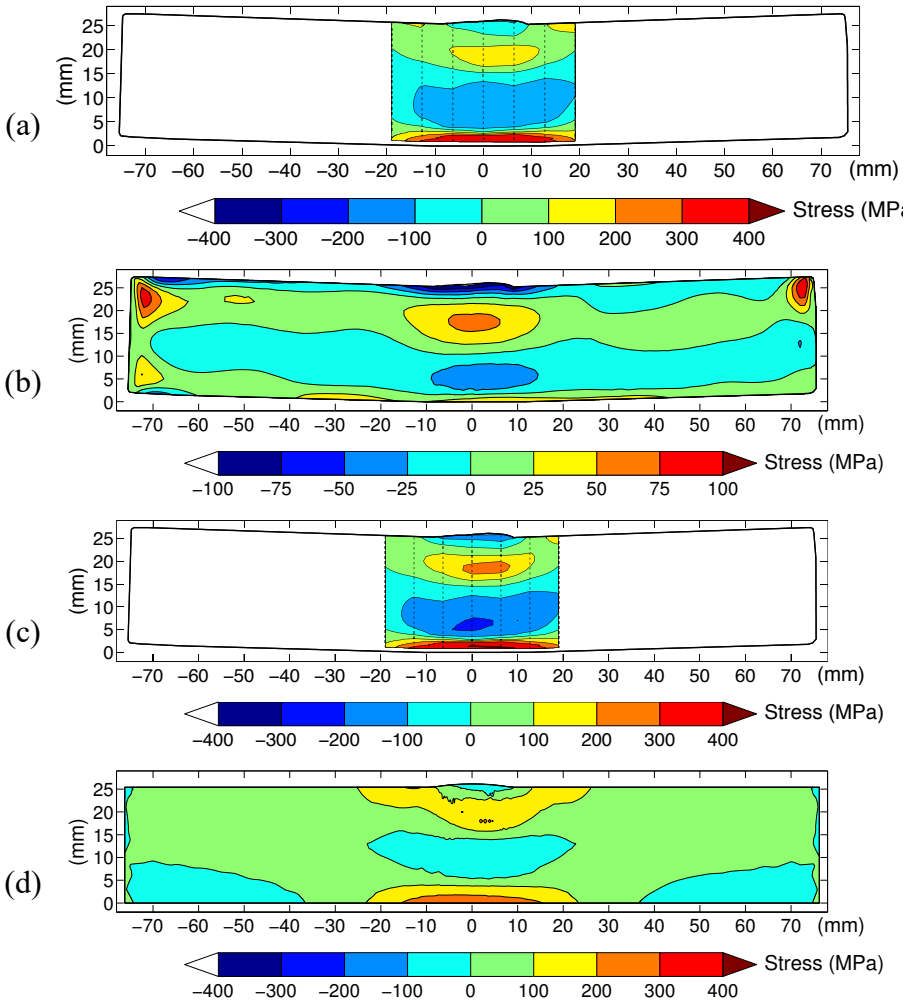

Fig. 11 – (a) Transverse stress remaining in slice (σ^C), (b) effect of longitudinal stress on transverse stress in the thin slice ($\sigma^{A(z)}$), (c) total transverse stress in original plate (σ^A), and (d) transverse stress from computational weld model

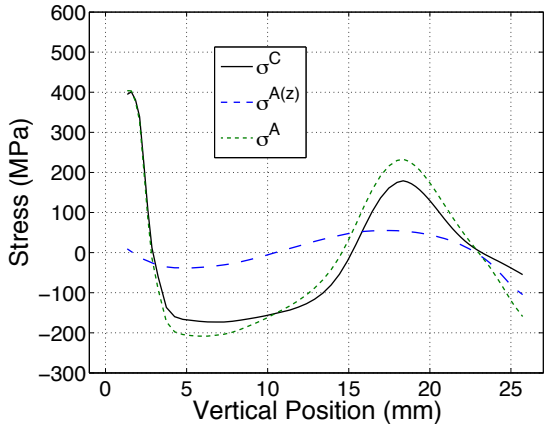

Fig. 12 – Plot of the transverse stresses at the weld center (x = 0) remaining in the slice (σ^C), effect of the longitudinal stress on the slice ($\sigma^{A(z)}$), and in original configuration (σ^A)

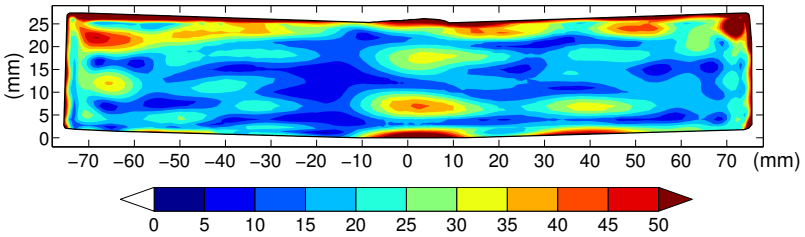

Fig. 13 – Uncertainty for the longitudinal stress (68% confidence interval)

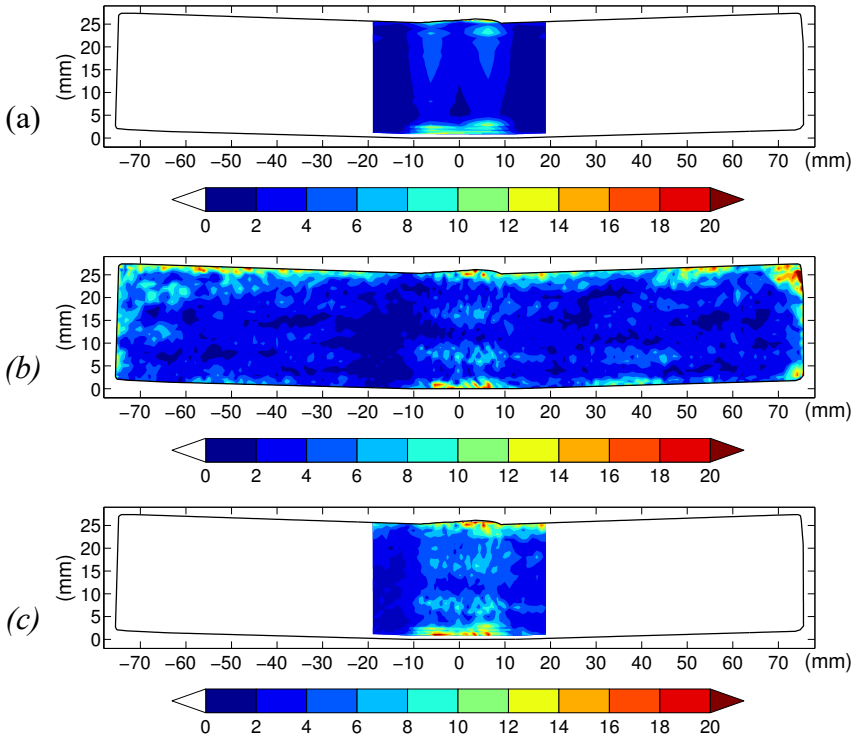

Fig. 14 – Uncertainty for the transverse stress (68% confidence interval) from (a) slitting measurement of stress remaining in slice (σ^{C}), (b) effect of longitudinal stress on transverse stress in the thin slice ($\sigma^{A(z)}$), and (c) total transverse stress uncertainty

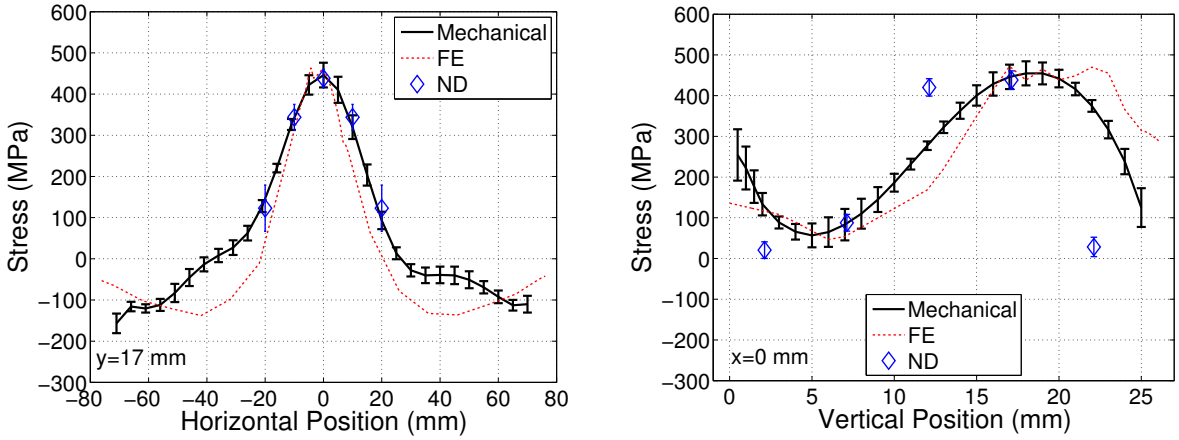

Fig. 15 – Line plots of the longitudinal stress found with present biaxial mapping, finite element weld simulation, and neutron diffraction along the (a) horizontal direction at y = 17 mm and (b) along the vertical at the weld center (x = 0)

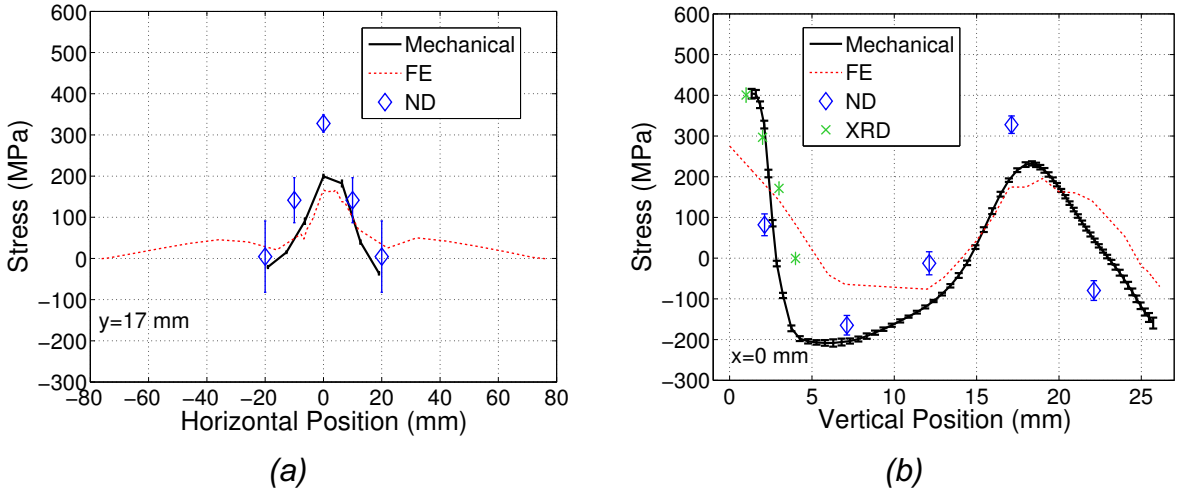

Fig. 16 – Line plots of the transverse stress found with biaxial mapping (Mechanical), finite element weld simulation (FE), and neutron diffraction (ND) along the (a) horizontal direction at y = 17 mm and (b) with x-ray diffraction (XRD) along the vertical at the weld center (x = 0). Note: XRD data have $\sigma^{A(z)}$ added to them to more easily compare the stresses in the plate (since the measurements were made in a slice)

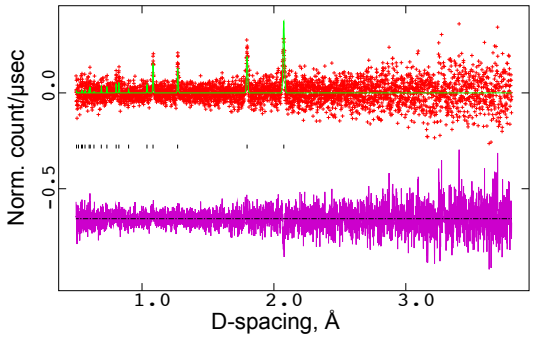

Fig. 17 – Typical neutron diffraction pattern for the stressed (d) sample. The red dots are the measured d-spacing, the green line is the Reitveld fit to the diffraction pattern, and the purple line is the difference between the measured and fit diffraction pattern